Structural ordering driven anisotropic magnetoresistance, anomalous Hall resistance and its topological overtones in full-Heusler Co_2MnSi thin films

Himanshu Pandey[1] and R. C. Budhani[1,2*]
[1] *Condensed Matter-Low Dimensional Systems Laboratory, Department of Physics, Indian Institute of Technology, Kanpur-208016, India.*
[2] *National Physical Laboratory, Council of Scientific and Industrial Research, New Delhi - 110012, India.**
(Dated: October 31, 2018)

We report the evolution of crystallographic structure, magnetic ordering and electronic transport in thin films of full-Heusler alloy Co_2MnSi deposited on (001) MgO with annealing temperatures (T_A). By increasing the T_A from 300°C to 600°C, the film goes from a disordered nanocrystalline phase to $B2$ ordered and finally to the $L2_1$ ordered alloy. The saturation magnetic moment improves with structural ordering and approaches the Slater-Pauling value of $\approx 5.0\mu_B$ per formula unit for $T_A = 600$°C. At this stage the films are soft magnets with coercive and saturation fields as low as $\approx$ 7 mT and 350 mT, respectively. Remarkable effects of improved structural order are also seen in longitudinal resistivity (ρ_{xx}) and residual resistivity ratio. A model based upon electronic transparency of grain boundaries illucidates the transition from a state of negative $d\rho/dT$ to positive $d\rho/dT$ with improved structural order. The Hall resistivity (ρ_{xy}) derives contribution from the normal scattering of charge carriers in external magnetic field, the anomalous effect originating from built-in magnetization and a small but distinct topological Hall effect in the disordered phase. The carrier concentration (n) and mobility (μ) have been extracted from the high field ρ_{xy} data. The highly ordered films are characterized by n and μ of 1.19× 10^{29} m^{-3} and 0.4 $cm^2V^{-1}s^{-1}$ at room temperature. The dependence of ρ_{xy} on ρ_{xx} indicates the dominance of skew scattering in our films, which shows a monotonic drop on raising the T_A. The topological Hall effect is analyzed for the films annealed at 300°C. We find maximum topological contribution to Hall resistivity around 0.5 T while it approach to zero with increasing magnetic field. The anisotropic magnetoresistance changes its sign from positive to negative as we go from as deposited to 600°C annealed film suggesting a gradual increase in the half-metallic character.

I. INTRODUCTION

Although discovered a century ago by F. Heusler, the compounds which bear his name have captured much attention in recent years due to their fascinating properties which include magneto-stuctural,[1] magneto-optical,[2] and magneto-caloric phenomena,[3] large thermo-electricity[4] and heavy fermion superconductivity.[5] Recently, a new property has been predicted in which spin-polarized edge and surface states are topologically protected against impurity scattering, known as topological insulator.[6,7] The coexistence of superconductivity and a magnetically ordered state have also been reported for Heusler alloys containing rare earth elements.[8] A certain class of full-Heusler alloys are particularly important for spintronics applications. The spin-polarized tunneling, which incorporates the imbalance between the density of states (DOS) of two spin states in the conduction band, controls the performance of devices like magnetic tunnel junctions and spin valves, and can be improved significantly if the conduction electrons are fully spin-polarized. These materials are characterized by a spin-split conduction band with a clear energy gap for the up and down spin states, and the Fermi level (ε_F) being located in one of them. This property of the electronic structure is called half-metallicity and a large number of Heusler alloys have been predicted to be half-metals. Although there are other compounds such as $La_{1-x}Sr_xMnO_3$[9] and CrO_2[10] with measured spin polarization > 90% at low temperatures, but they are not suitable for ambient temperature applications because of their low (< 400 K) Curie temperature (T_C). The Heusler alloys, which have very high T_C, are much suitable for spintronics applications, provided the spin-polarized nature of the conduction band can be retained in the films of these materials. However, due to atomic and/or antisite disorder, the degree for spin polarization in epitaxial films is found to be smaller than those obtained from various band structure calculations. Additionally, there is a reduction in spin polarization at the surfaces due to surface reconstruction,[11] and disorder[12] present between different sublattices. Therefore, studies of atomic and antisite disorder, surface reconstruction and spin polarization in thin films of Heusler alloys is a challenging but worthwhile problem to pursue.

Amongst all Heusler alloys, the Co-based full-Heusler compounds are attractive due to their high T_C and high magnetic moment per formula unit (f.u.). The full-Heusler alloy Co_2MnSi (CMS) belongs to the same family with $T_C = 985$ K[13] and a large minority-spin band gap of 0.4 eV. While, a large number of full-Heusler alloy thin films have been grown on semiconductors like Si,[14] Ge,[15] and GaAs;[16] there are few reports on the films grown on oxide substrates such as Al_2O_3,[17,18] MgO[18–20] and $SrTiO_3$.[21,22] Various deposition techniques such as laser ablation,[16,18,19,21–23] sputtering[24–27] and molecular beam epitaxy[28] are in use for the growth of such films under varying conditions of growth. It is well-known that the choice of the deposition temperature, growth conditions, and substrates can significantly alter the structural, magnetic, and electronic properties of thin films.

Here our focus is to carryout an in-depth study of the electronic transport and magnetism of CMS films grown on (001) MgO by a single target pulsed laser ablation technique (PLD). The lattice parameter ($a_{bulk} \approx$

0.5655 nm) of CMS matches quite well with the face diagonal ($\sqrt{2}a_{sub}$) of MgO. The lattice misfit [$(a - \sqrt{2}a_{sub})/\sqrt{2}a_{sub}$] between the CMS and MgO is $\approx -5\%$. It should be noted that the first principle calculations by Kandpal *et al.*[29] show that the strain $\approx \pm 5\%$ does not alter the band structure significantly. Thus, the charge transport in these films should behave in the same way as that of the bulk samples. The fabrication of stoichiometric films from an alloy target is the key strength of PLD. This technique relies on the formation of a local superheated region on the target, which then explodes as a plasmonic plume maintaining the stoichiometry of the target. The high thermal conductivity of elemental metals, however, hinders the formation of a superheated spot on the target and the material is removed by splashing, rather than ablation. Therefore, the parameters such as laser energy density, pulse repetition rate, and target-to-substrate distance need to be optimized very carefully.

The half-metallic character and saturation magnetization of Heusler alloys are linked to atomic structure and crystallographic ordering in the material. In thin films, the optimum realization of these two parameters is affected by lattice strain, interfacial metallurgy and surface roughness. The Heusler compound CMS crystallizes in the cubic space group $Fm\bar{3}m$ with $L2_1$ type ordering. This structure can be built from a zinc blende-type sublattice of one Co and one Si. The second Co fills the tetrahedral holes of the structure whereas Mn occupies the octrahedral holes. Theoretical calculations show that a small variation from this ordered arrangement of atoms can significantly affect the electronic and magnetic properties of the Heusler compounds. The greater atomic ordering is realized when the compound is synthesized at high temperatures. For electronic applications, it is desirable to grow films at as low a temperature as possible to ensure high surface smoothness and integration with other device process steps. Here we report the evolution of atomic ordering in CMS films deposited on (001) MgO at 200°C and subsequently annealed at several temperatures. The extent of atomic ordering has been monitored by two magneto-transport measurements; namely Anisotropic magnetoresistance (AMR) and Hall effect, which respectively yield quantitative information about the degree of spin polarization, saturation magnetization (M_S) and spin chirality. These data have been supported by direct measurement of magnetization, longitudinal resistivity and crystallographic structure. This paper comprises of following sections, out of which the introduction has been presented already in Sec. I. The sample preparation and various measurement procedures are given in Sec. II. All the results and their discussions are given in Sec. III, which deals with the structural and elemental characterization in addition to magnetic ordering and electronic transport in the CMS films. The anomalous Hall effect (AHE), topological Hall effect (THE), and AMR results are described in Sec. IV and finally, the conclusions drawn from these studies are given in Sec. V.

II. EXPERIMENTAL DETAILS

40 nm thick films of CMS were deposited by pulsed laser ablation of stoichiometric target of the alloy. A KrF excimer laser (wavelength = 248 nm and pulse width $\approx$ 20 ns) was used for the film deposition. The target was prepared by arc melting a mixture of the constituents (99.99% pure) in argon atmosphere. The alloy ingot was re-melted many times and then annealed at 1000^0C for 24 hours to secure homogenization. Prior to the annealing, the target was wrapped with tantalum foil in order to avoid any undesired oxidation and then placed in a quartz tube, which was subsequently evacuated and sealed. The resulting target has $L2_1$ structure and elemental stoichiometry in the ratio of 2:1:1 for Co, Mn, and Si, respectively as confirmed by X-ray diffraction (XRD) and energy dispersive X-ray analysis (EDAX). A Perfect site order can usually be achieved by preparing the films on lattice matched substrates at high temperatures. This is often undesirable for devices where requirement of smooth surfaces, sharp interfaces and minimized interdiffusion are the key for performance. We used a growth temperature of 200°C followed by one hour annealing at T_A = 300, 400, 500, and 600°C to enhance crystallization and ordering in the films. The growth and post-deposition annealing were carried out in an all-metal-seal high vacuum chamber equipped with a Ti-getter pump and an ultra high vacuum compatible substrate heater which could heat the samples to $\approx$ 850°C. Prior to the thin film deposition, the MgO substrates were annealed at 800°C for 30 minutes to allow surface reconstruction. Afterwards, the temperature was lowered to 200°C to commence the growth. The crystallographic structure of the films was characterized in θ-2θ, ω, φ, and grazing incidence X-ray diffraction (GIXRD) modes using a PANalytical X'Pert PRO X-ray diffractometer equipped with a Cu$K_{\alpha 1}$ source. From the simulation of X-ray reflectivity (XRR) curves by a genetic algorithm, we estimated the film thickness. The surface roughness of the films were obtained by XRR and atomic force microscopy (AFM). The high resolution field emission scanning electron microscopy (FESEM, Model: SUPRA40VP) and EDAX were used to check the homogeneity, stoichiometry and uniformity of the thin films. For room temperature magnetization measurements with both in-plane and out-of-plane field orientations, we have used a vibrating sample magnetometer. For the electrical measurements, samples were patterned in a four-probe geometry using Ar^+ ion milling through a stainless steel shadow mask and the silver pads for electrical contact were deposited by thermal evaporation. The resistivity and AMR measurement were performed in constant current mode using precision programmable dc current source (Keithley 224), digital temperature controller (Scientific Instruments Inc model 9650), and nanovoltmeter (Keithley 2182). For Hall measurement, samples were patterned into standard six probe Hall bar geometry and measured in Physical Property Measurement System (PPMS, Quantum Design).

III. RESULTS AND DISCUSSION

A. Structural and elemental characterization

The crystal structure of the ordered full-Heusler alloy CMS consists of four *fcc* sublattices with Co atoms at (1/4, 1/4, 1/4) and (3/4, 3/4, 3/4), the Mn atom at (0, 0, 0), and the Si atom at (1/2, 1/2, 1/2) in Wyckoff coordinates. These alloys are prone to antisite disorder. A complete disorder involving the mixing of all site, results in the $A2$ structure type with reduced symmetry $Im\bar{3}m$. The most frequently occuring disorder type is $B2$, where the Mn and Si atoms at $4a$ and $4b$ positions are interchanged randomly resulting in $Pm\bar{3}m$ symmetry. This type of disorder, in which the Co positions are not affected, changes the degree of spin polarization marginally.[30] Additionally, DO_3 disorder can take place, which consists of random exchange between Co and Mn atoms. Figure 1(a) shows the θ-2θ XRD profiles of CMS films annealed at different temperatures. The as-deposited film does not show any resolvable Bragg peaks suggesting a nano-crystalline nature. However, with the increase in T_A, the diffraction lines appear and their intensity and sharpness become prominent. The diffraction profile of 600°C annealed film shows intense (002) and (004) reflections of the cubic phase. The ratio of the intensities of the (002) and (004) Bragg peaks, which is a measure of the degree of crystallographic order on the Co sites,[31] also increases with T_A. Figure 1(b) shows the GIXRD spectra for 600°C annealed film taken to check the presence of (111) superlattice, that governs the ordering of the Mn and Si sublattices and (022) fundamental diffraction line, which confirms the presence of $L2_1$ ordering in the films. This is also earlier confirmed by taking the φ scans for (111) and (022) peaks of the CMS film.[19] The φ values for the (111) and (022) planes of the CMS film are shifted by 45^0 with respect to those of the MgO planes, clearly demonstrates the fourfold symmetry of cubic phase of 600°C annealed film. Rocking curves of the films have a full width at half maximum (FWHM) of $0.4^0 - 1.4^0$, indicating a high-quality epitaxial growth. A typical rocking curve about (004) CMS peak is shown in Fig. 1(c). The FWHM of these peaks decreases with the increase in T_A, which suggests that the (00ℓ) texture improves with increasing T_A. Figure 1(d) shows the variation of $B2$ and $L2_1$ ordering parameter with T_A calculated using the formulation given by Takamura *et al.*[32] These parameters give the measure of the atomic ordering in the ordered/diordered state of the Heusler alloys films.

The SEM micrographs of CMS films processed under different conditions are presented in Fig 2(a-c). These surfaces are devoid of any particulate matter, which is commonly seen in PLD grown films if the conditions are not optimized. We also note that the films become smoother as T_A increases. The non-contact AFM images of the above mentioned films are shown in Fig. 2(d-f). The roughness obtained from AFM scans and XRR measurements are compared in Fig. 2(g) (upper panel), while the lower panel shows the variation of grain size with T_A

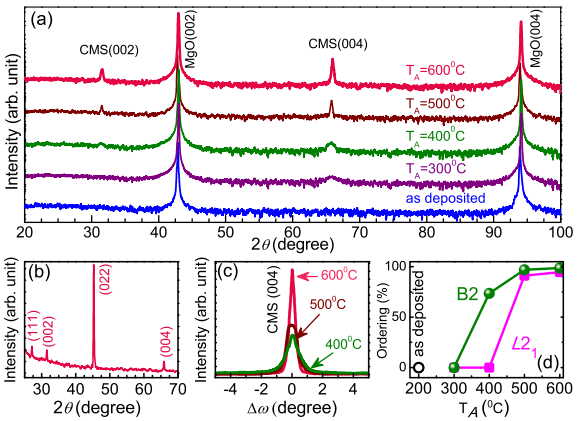

FIG. 1: (a) The θ-2θ X-ray diffraction patterns of 40 nm thick CMS films grown on MgO and subsequently annealed at different temperatures. The (002) and (004) peaks of CMS along with those of the substrates are marked. (b) GIXRD curve of CMS/MgO film annealed at 600°C confirming the presence of $L2_1$ ordering in the film. (c) The rocking curves for (004) peaks of CMS films for different T_A. (d) The variation of $B2$ and $L2_1$ structural ordering parameter with T_A.

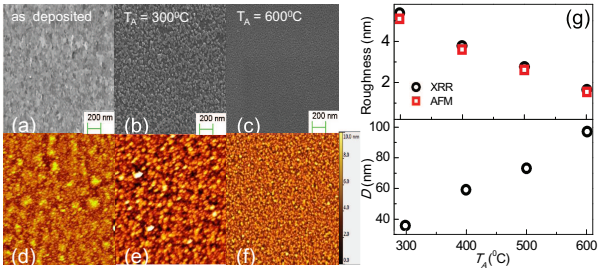

FIG. 2: (a-c) The SEM micrographs of CMS/MgO films for as-deposited, 300°C and 600°C annealed film. (d-f) The non-contact mode AFM images of the same films as shown in (a-c). The scan area is 5×5 μm^2. (g) The variation of film roughness (upper panel) and grain size (lower panel) with T_A.

estimated by using Debye-Scherrer method. As the T_A increases the grain size increase to attain (00ℓ) orientation.

In summary, these PLD grown films show three characteristically different structural states; (i) the as-prepared films having nanocrystalline phase with strong site disorder, (ii) the nanocrystalline phase with a substantial degree of site order inside the grains, and (iii) the crystalline phase with high degree of site order and structural long-range order.

B. Evolution of magnetic order on annealing

The magnetization (M) vs field (H) loops of the 600°C annealed film taken at room temperature in out-of-plane

and in-plane field directions are shown in Fig. 3(a). We clearly see that the films are magnetically soft with in-plane magnetization easy axis, coercive field (H_C) $\approx$ 7 mT, and almost square loops reaching saturation within 300 mT. The saturation magnetic moment extracted from these data is $\approx$ 4.78$\pm$0.19 μ_B/f.u., which is in accordance with the theoretical predictions.[33] The H_C of the films depends on the internal stresses, grain size, crystal structure, magnetic inhomogeneities, surface roughness, and thickness. The as-deposited film shows a much higher H_C compared to annealed films. The variation of H_C with T_A is shown in Fig. 3(b). The M_S of the films increases with the increasing T_A and approaches a maximum at 600°C for $L2_1$ ordered state [see Fig. 3(c)]. Clearly, increase in the structural disorder ($L2_1 \rightarrow B2 \rightarrow A2 \rightarrow$ amorphous state) causes reduction in M_S values. By using the M_S determined from hysteresis loops and out-of-plane saturation field H_K, one can calculate the perpendicular magnetic anisotropy energy density,

$$K = \int M \cdot dH = \int \left(M^{\perp} - M^{||} \right) \cdot dH \qquad (1)$$

which can be further simplified as $K = M_S H_K/2$. We obtained a K value of -5.82$\times 10^4$ J/m^3 for 600^{0}C annealed film, which is close to that obtained from ferromagnetic resonance measurement on such films.[19] The variation of K as a function of T_A is plotted in Fig. 3(d). We observe the K to be negative for all the films, implying an in-plane easy axis, which is consistent with the data shown in Fig. 3(a).

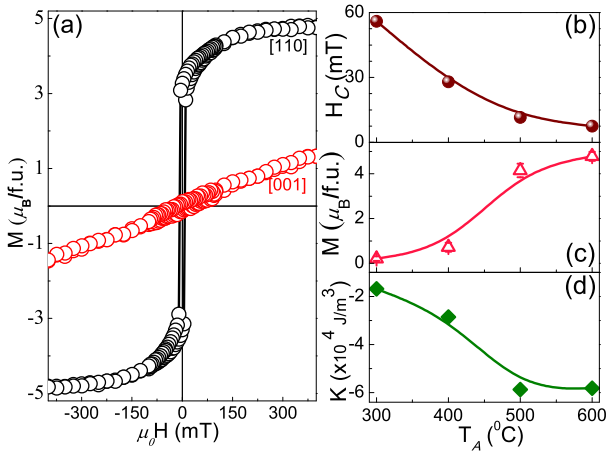

FIG. 3: (a) The room temperature magnetic hysteresis loops with external magnetic field $\mu_0 H$ applied along [110], and [001] CMS films annealed at 600°C. The variation of (b) coercivity, (c) saturation magnetization, and (d) perpendicular magnetic anisotropy constant with annealing temperature.

C. Reflection of atomic ordering on electronic transport

1. *Longitudinal resistivity* (ρ_{xx})

Now we describe the electrical transport in these PLD grown CMS films. Figure 4(a) shows the temperature dependence of longitudinal (ρ_{xx}) in zero field for the as-deposited films as well as for those annealed at 300, 400, 500, and 600°C. In the as-deposited state, the temperature coefficient ($d\rho/dT$) of resistivity is negative in the temperature range 5 K to 300 K with a residual resistivity ratio [$r = \rho_{300K}/\rho_{5K}$] of 0.8. This behavior is very unlike of a normal metal. The metallic nature of the films improves on annealing and a value of $r \approx 1.5$ is achieved after the heat treatment at 600°C, which is comparable with earlier reported values of r for CMS films.[25] The enhancement of r with the T_A is a result of the improvement in crystallographic ordering and, hence, a reduction of defect concentration in the film. The dependence of r and ρ_{xx} at 5 K with T_A are shown in the inset of Fig. 4(a). These data reveal that a distinctly metallic transport sets in only after annealing at $T_A >$ 300°C. In the case of disordered metals the resistivity becomes temperature independent when the elastic mean free path approaches the interatomic distances. This sets a limit on $\rho_{xx} \approx 150\mu\Omega$-cm, the so-called Mooji criterion,[34] often satisfied by metallic glasses, although large deviations are seen which suggests non-universality of this criterion. The resistivity of these films derives contributions from (i) the massive atomic disorder almost to the limit of being amorphous in as-grown films, (ii) transparency of grain boundaries whose number density decreases with increasing T_A, and (iii) the presence of antisite disorder. We believe that the huge changes in resistivity after annealing are primarily due to crystalline nature of the films and concomitant disorder at the large number of grain boundaries. We have examined our data using the grain boundary model proposed by Reiss *et al.*,[35] which can be viewed as a quantum correction to the classical Drude conductivity. This model attributes the reduced conductivity of the granular media to the number density and quantum transparency of grain boundaries crossed by an electron during two successive scattering events. In such scenario the effective mean free path is expressed as:

$$L_{eff} = L\gamma^{L/D} \qquad (2)$$

where L is the mean free path in the absence of granularity, γ is the transmission probability of the electrons through the grain boundary, and D is the grain size. The resistivity is thus written as:[36]

$$\rho(T) = \rho_{\infty}(T) \exp\left[\frac{A\kappa}{D\rho_{\infty}(T)}\right] \qquad (3)$$

where A = -lnγ, $\kappa = mv_F/ne^2$, $\rho_{\infty}(T) = \kappa/L$. The quantities m, v_F, and n are the mass, Fermi velocity, and density of conduction electrons, respectively. From Eq. (3), we can easily write the following relation:

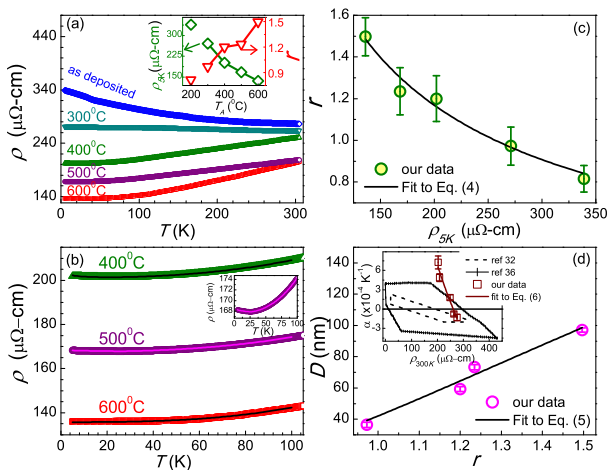

FIG. 4: (a) The resistivity of as-deposited film as well as the films annealed at various temperatures. The inset shows the variation of ρ_{5K} and r with T_A. (b) The $\rho(T)$ for the films annealed at 400, 500, and 600°C with their fits upto 100 K according to Eq. (7) shown by solid lines. The inset shows the low temperature upturn for 500°C annealed films. (c) The r as a function of ρ_{5K}. The continuous line represents the fit to experimental data using Eq. (4). (d) The D obtained from AFM measurements as a function of r with their fits using Eq. (5). The inset shows the variation of α_{300K} with ρ_{300K} with the fit according to Eq. (6).

$$r = r_\infty \left[\frac{\rho(5K)}{\rho_\infty(5K)}\right]^{(\frac{1}{r_\infty}-1)} \quad (4)$$

where $r_\infty = \rho_\infty(300K)/\rho_\infty(5K)$. In Fig. 4(c), the values of r for different films are reported as a function of ρ_{5K} along with the fitting of the data by using Eq. (4) with $r_\infty = (2.6 \pm 0.5)$ and $\rho_\infty(5K) = (53.6 \pm 9.3)\mu\Omega$-cm are well compared to the values obtained for single crystal CMS.[43] A high value of intra-grain room temperature resistivity $\rho_\infty(300K) = 140\mu\Omega$-cm compares in any case fairly well with the values reported in the literature.[37] We can also find a relation between r and D from Eq. (3) as follows:

$$\frac{r}{r_\infty} = \exp\left[\frac{A\kappa}{D\rho_\infty(5K)}\right]^{(\frac{1}{r_\infty}-1)} \quad (5)$$

Figure 4(d) shows the fit of the experimental data by the above expression, which gives the value of $A\kappa$ =(7.06±0.8)× 10^{-5} $\mu\Omega$-cm^2. Since we have κ= (3.55±0.62)×10^{-4} $\mu\Omega$-cm^2 for our CMS films, we get $\gamma = 0.82$ and hence a fairly strong coupling between the grains comes out even though the films have negative thermal coefficient of resistivity (TCR). The TCR is defined as $\alpha(T) = (1/\rho(T))/(d\rho(T)/dT)$, which can be written as:[36]

$$\alpha(T) = \alpha_\infty(T)\left[1 - \ln\left(\frac{\rho(T)}{\rho_\infty(T)}\right)\right] \quad (6)$$

where $\alpha_\infty(T) = \frac{1}{\rho_\infty(T)}\frac{d\rho_\infty(T)}{dT}$.

The α_{300K} calculated by fitting the data with Eq. (6), gives ρ_{300K}= (96.1±4.8)$\mu\Omega$-cm and α_∞(300K)= (25.7±3.2)×$10^{-4}K^{-1}$. Our values of α_{300K} for different films agree fairly well with the Mooij[34] and Tsuei[38] criterion.

Now, we move to discuss the resistivity of films which have positive TCR ($r > 1$). The $\rho(T)$ of a ferromagnetic metal film derives contributions from the defects, which is temperature independent, as well as from electron-electron scattering (e-e), one magnon scattering (1MS) and weak localization (WL) effects in the disordered phase. The $\rho(T)$ below $T < 100K$ can thus be expressed as

$$\rho(T) = \rho_0 + A_2T^2 + A_3T^3 + BT^{1/2} \quad (7)$$

where the coefficients A_2, A_3 and B corresponds to e-e, 1MS and WL processes. Here, we have ignored the T-linear electron-phonon scattering term, which is expected to dominate only for $T > 100K$. Generally, for half-metallic systems, the 1MS process is not possible due to absence of spin down states at ε_F. However, at finite temperature, the spin fluctuations in the minority bands can make a non-zero contribution to 1MS scattering. Furukawa has proposed that an unconventional 1MS can be possible, which leads to T^3 dependence of the resistivity.[39] The $BT^{1/2}$ term in Eq. (7) emulates a low temperature upturn seen in $\rho(T)$ of 400 and 500°C annealed film. The possible origin of this upturn is the weak localization due to e-e interaction effects, probably coming from the presence of impurities/disorder, or their combined effect with lattice dynamics. We found this upturn near 25 K for 500°C annealed film as shown in the inset of Fig. 4(b) and this minimum is not affected by the application of external magnetic field up to 0.3 T which negates the possibility of the well known Kondo-effect. A similar upturn in resistivity has been reported for Heusler alloys such as Ni_2MnGe,[40] CMS[24,41] and $Co_2Mn_xTi_{1-x}Al$.[42] To understand the effect of different scattering processes, we have fitted the resistivity curves below 100 K by using Eq. (7) and the fitting parameters are summarized in Table I with the error in second decimal place. From these parameters, one can find the relative weights of the respective resistivity components. The dominance of e-e scattering process is likely due to grain boundaries and dominates up to 35 K. At very low temperature, the magnetic scattering of quasiparticles is very small or nearly zero. Hence only e-e scattering would contribute to the resistivity the most. But, at some higher temperature the spin fluctuations near ε_F modify the electronic band structure and this may lead to 1MS scattering. The different behaviour of $\rho(T)$ curves and large variation in residual and room temperature resistivities and r in thin films as compared to those for bulk samples[43] of CMS could also be due to the significant contribution from the interface between the film and the substrate. This shows the importance of investigating the interface effects on the resistivity of these materials for fundamental and industrial point of view.

TABLE I: Fitting results of Eq. (7).

T_A	ρ_0	A_2	A_3	B	χ^2
°C	$\mu\Omega cm$	$\mu\Omega cmK^{-2}$	$\mu\Omega cmK^{-3}$	$\mu\Omega cmK^{-1/2}$	
400	202.9	9.31×10^{-4}	9.98×10^{-7}	-0.421	0.9999
500	169.1	7.51×10^{-4}	9.97×10^{-7}	-0.333	0.9999
600	135.8	6.34×10^{-5}	6.01×10^{-6}	0	0.9999

2. *Anomalous Hall Effect*

The Hall resistivity (ρ_{xy}) in ferromagnetic films provides valuable information about dominant carrier scattering mechanism, spin-orbit scattering, state of magnetization as well as non-trivial spin texture and their stability in H-T phase space. The ρ_{xy} of an inhomogeneous ferromagnet can be expressed as:

$$\rho_{xy} = R_0 H + R_S M_Z + \rho^{THE} \tag{8}$$

here the first term is the contribution from the Lorentz force experienced by the carriers in the presence of externally imposed magnetic field H. In the simple free electron model, $R_0 = 1/ne$, where n is the carrier concentration. The values for coefficient R_0 are obtained from the slope of ρ_{xy} data at high field range. The second term is the well known anomalous Hall effect (AHE), which derives contribution from the effect of spontaneous magnetization on scattering and a non-zero band average anomalous velocity transverse to the applied field.[44] The values of R_S for each temperature are obtained by extrapolating the ρ_{xy} data from the saturation value to zero magnetic field. The phenomenon of AHE has already been established by considering its extrinsic origin based on the skew scattering[45,46] and side jump mechanisms[47] on account of asymmetric scattering of spin-polarized charge carriers in the presence of spin-orbit interaction as well as the intrinsic origin, ascribed to Berry phase of Bloch electrons.[45–49] The anomalous Hall resistivity ($\rho^{AHE} = R_S M_Z$, M_Z is the magnetic moment measured along z direction) scales with the longitudinal resistivity (ρ_{xx}) as $\rho^{AHE} \propto \rho_{xx}^{\beta}$, where the exponent β varies from 1 to 2 depending on the strength of disorder. The topological Hall resisttivity (ρ^{THE}) evolves with the field, which affects the inhomogeneous spin texture in a non-trivial manner; but reduces to zero at high fields beyond saturation of magnetization.

Figure 5 shows $\rho_{xy}(H)$ data measured at different temperatures for the CMS films. Below saturation, ρ_{xy} is governed by the AHE and increases with the increase in the sample magnetization. Like ρ_{xx}, the ρ_{xy} decreases with decreasing temperature and becomes almost constant below 20 K. The low temperature values of ρ_{xy} changes with the T_A. For the films annealed at 600°C, the ρ_{xy} is close to zero, whereas, in 500°C annealed film, the ρ_{xy} gains a negative values due to DO_3 disorder and finally, it attains a positive values for 400 and 300°C annealed samples on account of higher degree of $B2$ disorder.

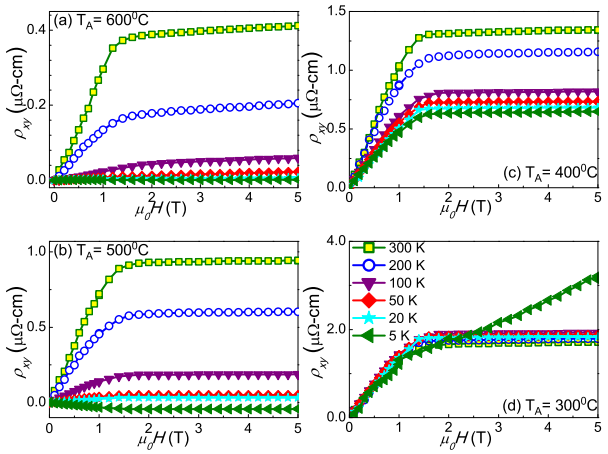

FIG. 5: Hall measurements of CMS films annealed at various temperatures (a) 600, (b) 500, (c) 400, and (d) 300°C.

Figure 6(a) shows the carrier concentration (n) of CMS films as a function of temperature for different T_A values. The Hall mobility (μ) $= \sigma_{xx}/ne$ remains nearly constant as shown in Fig. 6(b). The film annealed at 600°C is characterized by n and μ of $1.19\times\ 10^{29}$ m^{-3} and 0.4 cm$^2V^{-1}s^{-1}$, respectively measured at room temperature. Our values of n and μ are comparable to previously reported studies on MgO.[20]

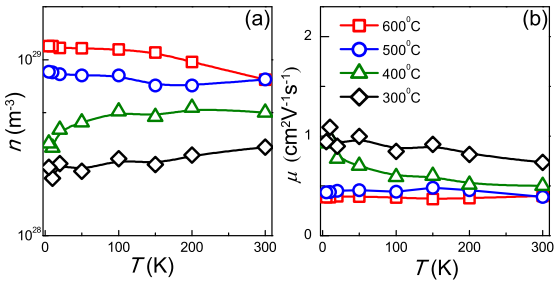

FIG. 6: The variation of (a) carrier concentration and (b) electron mobility with temperature for CMS films annealed at different temperatures.

The scaling between ρ^{AHE} and ρ_{xx} is an important issue for better understanding of AHE. This correlation suggests the presence of dominant scattering mechanisms in both resistivities ρ_{xy} responsible for the appearance of AHE phenomenon caused by defects and antisite disorder.[50] In general, we have,

$$\rho^{AHE} = a\rho_{xx} + b\rho_{xx}^2 \tag{9}$$

where the coefficients a and b give the proportions of skew scattering, side-jump and the intrinsic mechanisms. Figure 7(a) shows the variation of ρ^{AHE} with ρ_{xx} for various films, whereas, the temperature dependence of ρ^{AHE} is shown in Fig. 7(b). This also follows as the behaviour with respect to temperature as for ρ_{xx}. So $\rho^{AHE}(T)$ can be separated into temperature-independent

$[\rho^{AHE}(0)]$ and temperature-dependent $[\rho^{AHE}(T)]$ resistivity below 20 K. Hence, Eq. (9) can be rewrittten as:

$$\rho^{AHE}(T) = \rho^{AHE}(0) + [a + 2b\rho_{xx}(0)]\rho_{xx}(T) + b\rho_{xx}^2(T) \quad (10)$$

where $\rho^{AHE}(0) = a\rho_{xx}(0) + b\rho_{xx}^2(0)$ is the residual anomalous Hall resistivity. By substracting ρ^{AHE} values at two different temperatures, we can separate the temperature dependent part. Hence, Eq. (10) will be reformed as:

$$\Delta\rho^{AHE} = [a + 2b\rho_{xx}(0)]\Delta\rho_{xx}(T) + b\Delta[\rho_{xx}^2(T)] \quad (11)$$

Here we have taken the difference in the resistivities with respect to the values at 20 K and plotted in Fig. 7(c) with fitting in according to Eq. (11). We find a linear dependence for all the films with different slopes except for 300°C annealed films. The slopes of the lines decrease with increase in T_A as the skew scattering term (a) decreases where as the scattering independent term (b) increases as shown in Fig. 7(d). These two fitting parameters decide the dominance of the scattering present in the films. The values for a and b are $(6\pm1)\times10^{-3}$ and $(2.39\pm0.26)\times10^{-6}$ $\mu\Omega^{-1}$cm^{-1}, respectively for $L2_1$ ordered 600°C annealed film and we found $[a + 2b\rho_{xx}(0)] > b\rho_{xx}(0)$ with $\rho_{xx}(0) \approx 135.8$ $\mu\Omega$-cm. This clearly suggests the dominance of linear scaling due to skew-scattering mechanism. The values of these fitting parameters change very drastically as we change T_A. So the structural ordering as well as magnetization in addition to other factors like impurities in the films and their thermal history are the important constituents which affect the scattering mechanism in the films.

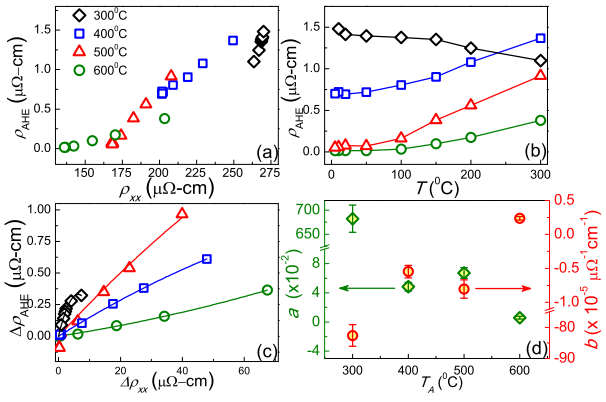

FIG. 7: (a) The variation of ρ^{AHE} with ρ_{xx} for CMS films annealed at different temperatures. (b) The temperature dependence of ρ^{AHE}. (c) $\Delta\rho^{AHE}$ against $\Delta\rho_{xx}(T)$ with the fit of the data according to Eq. (11). (d)The linear (left ordinate) and quadratic (right ordinate) fitting parameters with varying T_A.

3. *Topological Hall Effect*

Now we discuss the THE, which emerges due to inhomogeneous spin textures in the presence of magnetic field, but reduces to zero at very high field. The film annealed at 300°C may show a non trivial spin character as it contains sufficient amount of antisite disorder as well as smaller grain size, which can lead to inhomogeneous magnetization. The canting of the magnetic spins makes the magnetization of the 300°C annealed films depart from in-plane easy axis. The possibility of minority spins at ε_F also allows the scattering between spin-up and spin-down carriers. Hence, the spin canting and presence of minority spins at ε_F may show some signatures of THE in 300°C annealed films at low temperature. The ρ^{THE} can be obtained by subtracting the $(R_0H + R_SM_Z)$ from ρ_{xy}. The experimental ρ_{xy} data measured at 5 K for 300°C annealed film along with the calculated $(R_0H + R_SM_Z)$ values and ρ^{THE}, are shown in Fig. 8. The ρ_{xy} and $(R_0H + R_SM_Z)$ increase monotonically with H and coincide at high magnetic fields suggesting a diminishing effect of ρ^{THE}. The contribution of ρ^{THE} shows a minima around 0.5 T. This type of behaviour has been observed in previous experiments[51–53] and described in theories.[54] The inset of Fig. 8 shows a systematic variation of normalized topological Hall resistivity $[\xi{=}\rho^{THE}/\rho_{xy}(14T)]$ for differently annealed films to understand the effect of disorder on ρ^{THE}. The films annealed at 500 and 600°C do not show any THE due to strong magnetic coupling, robust uniaxial in-plane anisotropy, and a half-metallic character. As the T_A reduced to 300°C, a minimum in the ξ occurs. This observation shows that the inhomogeneous magnetization which contribute to ρ^{THE} diminishes as the films become more ordered.

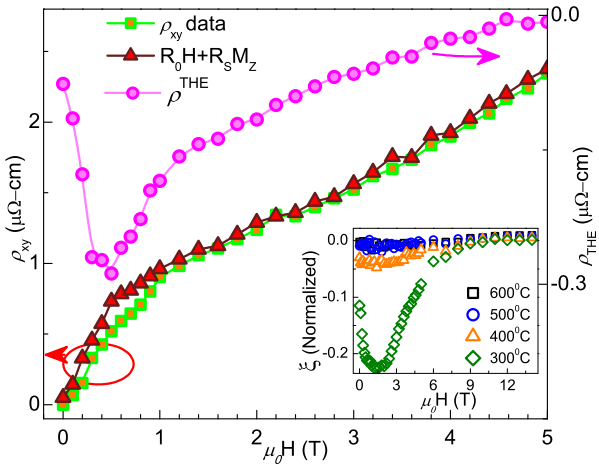

FIG. 8: Hall resistivity measured at 5 K as a function of field for 300°C annealed film. The inset shows the normalized topological Hall resistivity for films annealed at different temperature.

4. *Anisotropic magnetoresistance*

Ferromagnetic materials show a distinct contribution ρ_{xx} that depends on the direction of magnetization with respect to the direction of the current used to measure ρ_{xx}. This effect, commonly known as Anisotropic mag-

netoresistance (AMR), arises from spin-orbit interaction and is of significant technological and fundamental interest. The AMR is defined as;

$$\frac{\Delta\rho}{\rho} = \frac{\rho_{||} - \rho_{\perp}}{\rho_{\perp}}, \tag{12}$$

where $\rho_{||}(\rho_{\perp})$ represents the resistivity when the current flows parallel (perpendicular) to the magnetization. The original work of Cambell *et al.* attributes AMR to *s-d* scattering from the conduction states and successfully explains the AMR data of crystalline $3d$ transition metal alloys.[55] A further improvement of the theory by Malozemoff takes into account the *s-s* scattering as well,[56] but these models do not consider the spin polarization of *s*-states. Kokado *et al.* have shown that when the dominant *s-d* scattering process occurs between those states which have same type of spin, the AMR ratio is negative ($\rho_{||} < \rho_{\perp}$), and when the dominant scattering occurs between opposite spin states, the sign tends to be positive.[57] This prediction has a special significance for the half-metallic systems as they have only one type of spin states at ε_F, and hence, should show a predominantly negative AMR. We have measured the AMR of our films in a field strength of ≤ 0.3 T, which is sufficient to saturate the magnetization.

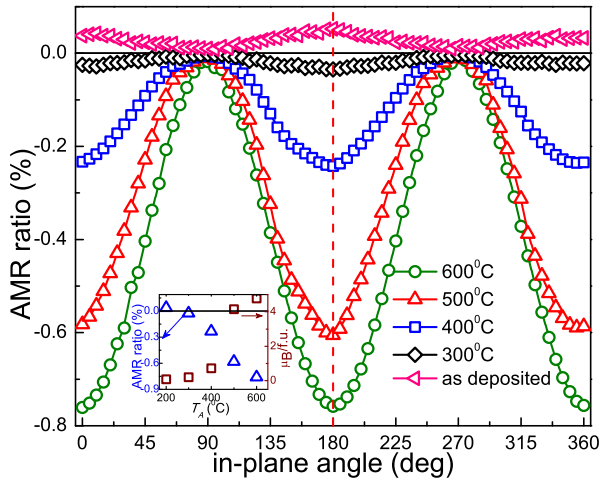

FIG. 9: Dependence of the AMR ratio on the in-plane relative angle (ϕ) between direction of applied current and magnetic field for CMS films measured at 7 K. Inset shows the variation of AMR ratio and magnetic moment with T_A.

Figure 9 shows the dependence of the AMR ratio on the angle ϕ between the current and external field for CMS films measured at 7 K, where the AMR ratio is defined as $[(R(\phi) - R_{\perp})/R_{\perp}]$, where $R_{\perp}$ corresponds to $\phi = 90°$. The obtained values of AMR ratios are comparable with the earlier reports on mangnites[58,59] and full-Heusler alloy $Co_2Fe_xMn_{1-x}Si$.[60] Our data show a twofold symmetry for all the films with minimum occurring at ϕ= 0° and 180°, showing negative AMR values. The magnitude of the AMR increases with the T_A (see the inset of Fig. 9) and changes its sign for highly disordered as-deposited film suggesting changes in the DOS at ε_F and the degree of spin polarization due to increasing structural disorder. These observation indicates that even though the film annealed at 400°C exhibits half-metallic character with $B2$ ordering, there must be some overlap between ε_F and the minority band which decreases further on raising the T_A due to improvement of structural ordering.

IV. CONCLUSIONS

In summary, we prepared laser ablated thin films of Co_2MnSi with different degree of disorder realized by post-deposition annealing in the temperature range of 300 to 600°C. In the as-deposited state, the film is composed of nano-crystalline grains with $A2$ type disorder. The film behaves as a strongly disordered metal with negative TCR due to the scattering from grain boundaries and the site disorders within the grains. Annealing improves structural ordering from disordered nanocrystalline to $B2$ phase and finally highly ordered $L2_1$ phase is obtained at 600°C. The system becomes metallic with positive TCR for $T_A > 300$°C. The saturation magnetization builds up on annealing and reaches the bulk value as predicted by Slater-Pauling rule at $T_A = 600$°C. The behaviour of TCR, room temperature resistivity and residual resistivity ratio are analyzed in the framework of a model based on quantum transparency of grain boundaries. These results establish three structural states in our films, the as-prepared nanocrystalline phase with strong site disorder, an intermediate phase with a small amount of site order inside the grains, and the crystalline phase with long-range structural order. A systematic study of anomalous Hall effect reveals the experimental evidence of skew-scattering phenomena. We also observed an overtone of topological Hall effect in our strongly disordered nano-crystalline 300°C annealed films which vanishes at higher magnetic fields. The normalized value of topological Hall resistivity (ξ) is almost zero for 500 and 600°C annealed films. We found a maximum value of $\xi \approx 0.22$ for 300°C annealed film. The annealing temperature dependence of the THE suggests the canting and/or texturing of spins in the films annealed at 300°C. An AMR ratio of ≈ -0.76% is obtained for 600°C annealed film, which decreases sharply as T_A reduces, whereas, we found AMR of ≈0.04 for as-deposited film. This small positive value of AMR suggests disappearance of half-metallicity.

V. ACKNOWLEDGEMENT

This research has been supported by Council for Scientific and Industrial Research (CSIR), Government of India. H.P. would like to thank V. P. S. Awana for directing him to use the PPMS. He also thanks the DST Unit on Nanosciences (IIT Kanpur) for the SEM and GIXR measurements and acknowledges financial support from Indian Institute of Technology Kanpur and CSIR. R.C.B. acknowledges J. C. Bose Fellowship of the Department of

Science and Technology, Govt. of India.

* Electronic address: rcb@iitk.ac.in, rcb@nplindia.org

[1] R. Kainuma, Y. Imano, W. Ito, H. Morito, S. Okamoto, O. Kitakami, K. Oikawa, A. Fujita, T. Kanomata, and K. Ishida , Nature **439**, 957 (2006).

[2] T. Krenke, E. Duman, M. Acet, E. F. Wassermann, X. Moya, L. Mañosa, and A. Planes, Nat. Mat. **4**, 450 (2005).

[3] P. G. van Engen, K. H. J. Bushow, R. Jongebreuer, and M. Erman, Appl. Phys. Lett. **42**, 202 (1983).

[4] S. Bosu, Y. Sakuraba, K. Uchida, K. Saito, T. Ota, E. Saitoh, and K. Takanashi, Phys. Rev. B **83**, 224401 (2011).

[5] J. H. Wernick, G. W. Hull, T. H. Geballe, J. E. Bernadini, and J. V. Waszczak, Mater. Lett. **2**, 90 (1983).

[6] S. Chadov, X. Qi, J. Kübler, G. H. Fecher, C. Felser, and S. C. Zhang, Nat. Mat. **9**, 541 (2010).

[7] H. Lin, L. A. Wray, Y. Xia, S. Xu, S. Jia, R. J. Cava, A. Bansil, and M. Z. Hasan, Nat. Mat. **9**, 546 (2010).

[8] H. A. Kierstead, B. D. Dunlap, S. K. Malik, A. M. Umarji, and G. K. Shenoy, Phys. Rev. B **32**, 135 (1985).

[9] J. H. Park, E. Vescovo, E. Kim, C. Kwon, R. Ramesh, and T. Venkatesan, Nature **392**, 794 (1998).

[10] Y. Ji, G. J. Strijkers, F. Y. Yang, C. L. Chien, J. M. Beyers, A. Anguclouch, G. Xiao, and A. Gupta, Phys. Rev. Lett. **86**, 5585 (2001).

[11] D. Ristoiu, J. P. Nozières, C. N. Borca, B. Borca, and P. A. Dowben, Appl. Phys. Lett. **76**, 2349 (2000).

[12] M. C. Kautzky, F. B. Mancoff, J. F. Bobo, P. R. Johnson, R. L. White, and B. M. Clemens, J. Appl. Phys. **81**, 4026 (1997).

[13] S. Fujii, S. Sugimura, Ishida, and S. Asano, J. Phys: Con. mat. **2**, 8583 (1990).

[14] M. Zander, J. Herfort, K. Kumakura, H-P Scöhnherr, and A. Trampert, J. Phys. D: Appl. Phys. **43**, 305004 (2010).

[15] K. Kasahara, K. Yamamoto, S. Yamada, T. Murakami, K. Hamaya, K. Mibu, and M. Miyao, J. Appl. Phys. **107**, 09B105 (2010).

[16] W. H. Wang, M. Przybylski, W. Kuch, L. I. Chelaru, J. Wang, Y. F. Lu, J. Barthel, H. L. Meyerheim, and J. Kirschner, Phys. Rev. B **71**, 144416 (2005).

[17] L. J. Singh, Z. H. Barber, Y. Miyoshi, Y. Bugoslavsky, W. R. Branford, and L. F. Cohen, Appl. Phys. Lett. **84**, 2367 (2004).

[18] H. Schneider, G. Jakob, M. Kallmayer, H. J. Elmers, M. Cinchetti, B. Balke, S. Wurmehl, C. Felser, M. Aeschlimann, and H. Adrian, Phys. Rev. B **74**, 174426 (2006).

[19] H. Pandey, P. C. Joshi, R. P. Pant, R. Prasad, S. Auluck, and R. C. Budhani, J. Appl. Phys. **111**, 023912 (2012).

[20] H. Schneider, E. Vilanova, B. Balke, C. Felser, and G. Jakob, J. Phys. D Appl. Phys. **42**, 084012 (2009).

[21] Anupam, P. C. Joshi, P. K. Rout, Z. Hossain and R. C. Budhani, J. Phys. D: Appl. Phys. **43**, 255002 (2010).

[22] V. Toutam, H. Pandey, S. Singh, and R. C. Budhani, AIP ADVANCES **3**, 022124 (2013).

[23] P. K. Rout, H. Pandey, Anupam, P. C. Joshi, Z. Hossain, and R. C. Budhani, manuscript submitted.

[24] U. Geiersbach, A. Bergmann, and K. Westerholt, J. Mag. Mag. Mat. **240**, 546 (2002).

[25] M. P. Raphael, B. Ravel, Q. Huang, M. A. Willard, S. F. Cheng, B. N. Das, R. M. Stroud, K. M. Bussmann, J. H. Claassen, and V. G. Harris, Phys. Rev. B **66**, 104429 (2002).

[26] S. Kämmerer, A. Thomas, A. Hütten, and G. Reiss, Appl. Phys. Lett. **85**, 79 (2003).

[27] K. Kim, S. J. Kwon, and T. W. Kim, Phys. Status Solidi B Basic Res. **241**, 1557 (2004).

[28] T. Ambrose, J. J. Krebs, and G. A. Prinz, Appl. Phys. Lett. **76**, 3280 (2000).

[29] H. C. Kandpal, G. H. Fecher, C. Felser, and G. Schönhense, Phys. Rev. B **73**, 094422 (2006).

[30] Y. V. Kudryavtsev, V. N. Uvarov, V. A. Oksenenko, Y. P. Lee, J. B. Kim, Y. H. Hyun, K. W. Kim, J. Y. Rhee, and J. Dubowik, Phys. Rev. B **77**, 195104 (2008).

[31] P. J. Webster, J. Phys. Chem. Solids **32**, 1221 (1971); K. R. A. Ziebeck and P. J. Webster, J. Phys. Chem. Solids **35**, 1 (1974).

[32] Y. Takamura, R. Nakane, and S. Sugahara, J. Appl. Phys. **105**, 07B109 (2009).

[33] I. Galanakis, P. H. Dederichs, and N. Papanikolaou, Phys. Rev. B **66**, 174429 (2002).

[34] J. H. Mooij, Phys. Status Solidi A **17**, 521 (1973).

[35] G. Reiss, J. Vancea, and H. Hoffmann, Phys. Rev. Lett. **56**, 2100 (1986).

[36] A. Nigro, G. Nobile, M. G. Rubino, and R. Vaglio, Phys. Rev. B **37**, 3970 (1988).

[37] K. Senapati, N. K. Pandey, Rupali Nagar, and R. C. Budhani, Phys. Rev. B **74**, 104514 (2006).

[38] C. C. Tsuei, Phys. Rev. Lett. **57**, 1943 (1986).

[39] N. Furukawa, J. Phys. Soc. Jpn. **69**, 1954 (2000).

[40] M. S. Lund, J. W. Dong, J. Lu, X. Y. Dong, C. J. Palmstrøm, and C. Leighton, Appl. Phys. Lett. **80**, 4798 (2002).

[41] L. J. Singh, Z. H. Barber, Y. Miyoshi, W. R. Branford, and L. F. Cohen, J. Appl. Phys. **95**, 7231 (2004).

[42] M. Aftab, G. H. Jaffari, S. K. Hasanain, T. A. Abbas, and S. I. Shah, J. Phys. D: Appl. Phys. **45**, 475001 (2012).

[43] L. Ritchie, G. Xiao, Y. Ji, T. Y. Chen, C. L. Chien, M. Zhang, J. Chen, Z. Liu, G. Wu, and X. X. Zhang, Phys. Rev. B **68**, 104430 (2003).

[44] N. Nagaosa, J. Sinova, S. Onoda, A. H. MacDonald, and N. P. Ong, Rev. Mod. Phys. **82**, 1539 (2010).

[45] J. M. Luttinger and W. Kohn, Phys. Rev. **97**, 869 (1955).

[46] J. Smit, Physica **24**, 39 (1958).

[47] L. Berger, Phys. Rev. B **2**, 4559 (1970).

[48] R. Karplus and J. M. Luttinger, Phys. Rev. **95**, 1154 (1954).

[49] M. V. Berry, Proc. R. Soc. London, Ser. A**392**, 45 (1984).

[50] E. V. Vidal, H. Schneider, and G. Jakob, Phys. Rev. B **83**, 174410 (2011).

[51] N. Kanazawa, Y. Onose, T. Arima, D. Okuyama, K. Ohoyama, S. Wakimoto, K. Kakurai, S. Ishiwata, and Y. Tokura, Phys. Rev. Lett. **106**, 156603 (2011).

[52] A. Neubauer, C. Pfleiderer, B. Binz, A. Rosch, R. Ritz, P. G. Niklowitz, and P. Böni, Phys. Rev. Lett. **102**, 186602 (2009).

[53] M. Lee, W. Kang, Y. Onose, Y. Tokura, and N. P. Ong, Phys. Rev. Lett. **102**, 186601 (2009).

[54] S. D. Yi, S. Onoda, N. Nagaosa, and J. H. Han, Phys. Rev. B **80**, 054416 (2009).

[55] I. A. Campbell, A. Fert, and O. Jaoul, J. Phys. C: Solid State Phys. **3** (Metal Phys. Suppl.) S**95** (1970).

[56] A. P. Malozemoff, Phys. Rev. B **32**, 6080 (1985).

[57] S. Kokado, M. Tsunoda, K. Harigaya, and A. Sakuma, J. Phys. Soc. Jpn. **81**, 024705 (2012).

[58] M. Ziese, Phys. Rev. B **62**, 1044 (2000); M. Ziese and S. P. Sena, J. Phys. Con. Mat. **10**, 2727 (1998).
[59] E. Favre-Nicolin and L. Ranno, J. Magn. Magn. Mater. **272**, 1814 (2004).
[60] F. J. Yang, Y. Sakuraba, S. Kokado, Y. Kota, A. Sakuma, and K. Takanashi, Phys. Rev. B **86**, 020409(R) (2012).